Liang *et al. Biochar* (2024) 6:41
https://doi.org/10.1007/s42773-024-00331-4

Biochar

ORIGINAL RESEARCH Open Access

Roles of iron and manganese in bimetallic biochar composites for efficient persulfate activation and atrazine removal

Yuan Liang[1*], Ran Tao[1], Ben Zhao[1], Zeda Meng[2], Yuanyuan Cheng[1], Fan Yang[3], Huihui Lei[1] and Lingzhao Kong[1*]

Abstract

As for Atrazine ($C_8H_{14}ClN_5$) degradation in soil, iron (Fe)-manganese (Mn) bimetallic biochar composites were proved to be more efficient for persulfate (PS) activation than monometallic ones. The atrazine removal rates of Fe/Mn loaded biochar + PS systems were 2.17–2.89 times higher than Fe/Mn loaded biochar alone. Compared with monometallic biochar, the higher atrazine removal rates by bimetallic biochar (77.2–96.7%) were mainly attributed to the synergy degradation and adsorption due to the larger amounts of metal oxides on the biochar surface. Atrazine degradation in Fe-rich biochar systems was mainly attributed to free radicals (i.e., $SO_4^{\cdot-}$ and ·OH) through oxidative routes, whereas surface-bound radicals, $^1O_2$, and free radicals were responsible for the degradation of atrazine in Mn-rich biochar systems. Furthermore, with a higher ratio of Fe(II) and Mn(III) formed in Fe-rich bimetallic biochar, the valence state exchange between Fe and Mn contributed significantly to the more effective activation of PS and the generation of more free radicals. The pathways of atrazine degradation in the Fe-rich bimetallic biochar systems involved alkyl hydroxylation, alkyl oxidation, dealkylation, and dechlorohydroxylation. The results indicated that bimetallic biochar composites with more Fe and less Mn are more effective for the PS-based degradation of atrazine, which guides the ration design of easily available carbon materials targeted for the efficient remediation of various organic-polluted soil.

Highlights

- Both Fe- and Mn-rich bimetallic biochar can effectively activate persulfate, but Fe-rich biochar is superior.
- Atrazine degradation in Fe-rich biochar systems was attributed to free radicals through oxidative routes.
- Atrazine degradation pathways involved alkyl hydroxylation, alkyl oxidation, dealkylation, and dechlorohydroxylation.

Keywords Atrazine, Bimetallic biochar composites, Persulfate, Radicals, Non-radicals, Degradation pathways

Handling editor: Xiangzhou Yuan.

*Correspondence:
Yuan Liang
liangyuan@usts.edu.cn
Lingzhao Kong
konglz@sari.ac.cn
Full list of author information is available at the end of the article

Graphical Abstract

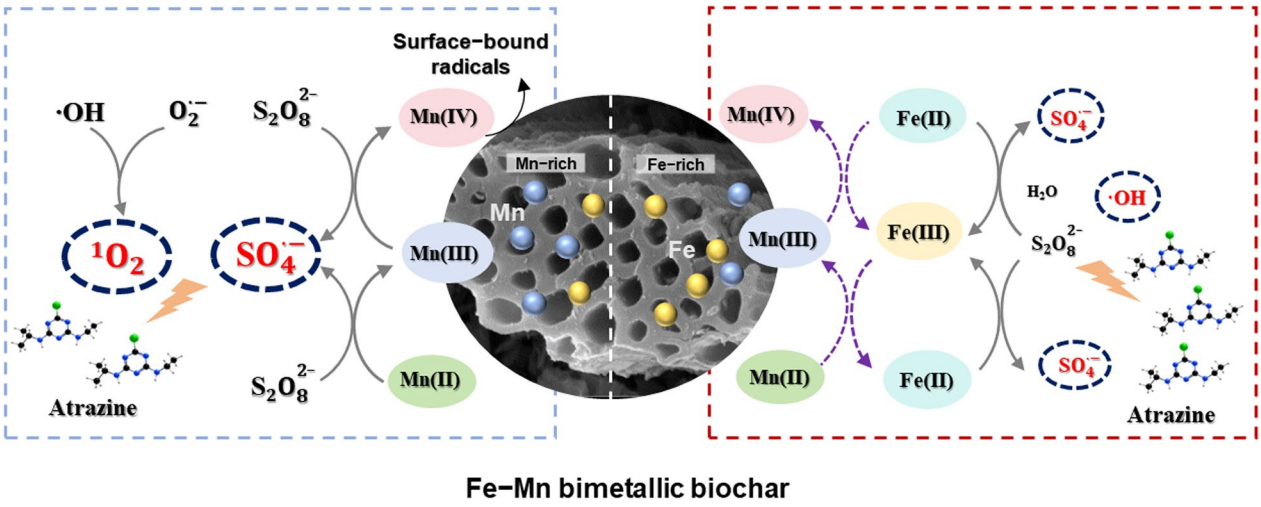

1 Introduction

Atrazine ($C_8H_{14}ClN_5$) is the most widely used herbicide in the world (Bohn et al. 2011). About 70,000–90,000 tons of atrazine were applied annually in the world (Ta et al. 2006), and 29,000–33500 tons were used in agriculture in the US in 2012 (Gaffar et al. 2021). Due to its widespread use, stable structure (Bessac et al. 2013), and low adsorption by soil (Kolekar et al. 2019), atrazine in agricultural soil easily migrates to groundwater and surface water through rainwater or irrigation. The concentration range of atrazine in the environment is very wide. For example, the atrazine concentration investigated in groundwater was 0.068 μg L^{-1} in western Germany (Vonberg et al. 2014). The concentration of atrazine was 0.02–0.10 mg Kg^{-1} in topsoil of agricultural areas in Serbia (Gasic et al. 2002), but the atrazine concentration of industrial wastewater could higher than 10 mg L^{-1}. It can also accumulate in plants, animals, and even humans through the food chain. Atrazine, even at low concentrations, is an endocrine disruptor, posing a potential risk to humans and other organisms (Luo et al. 2019; Yan et al. 2015). Therefore, effective measures must be taken to remove residual atrazine from the environment.

Advanced oxidation processes have a high efficiency in decomposing organic pollutants (Giannakopoulos et al. 2022). For example, hydroxyl radical (·OH) showed high efficiency in wastewater treatment (Zhu et al. 2023). However, persulfate (PS) has attracted more significant attention in environmental remediation (Shan et al. 2020), and showed the following advantages over hydroxyl radical (·OH)-based methods: (1) The redox potential of sulfate radical ($SO_4^{\cdot-}$) is higher than that of ·OH (E_0 2.5–3.1 vs 2.7–2.8 eV) (Asghar et al. 2015); (2) $SO_4^{\cdot-}$ demonstrates better selectivity and more thorough degradation of organic pollutants (Han et al. 2015); (3) $SO_4^{\cdot-}$ has a longer lifetime (4 s) compared to ·OH (with a lifetime of < 1 s), significantly increasing the contact time with organic pollutants (Xiao et al. 2018). However, the spontaneous generation of $SO_4^{\cdot-}$ by PS alone is challenging, rendering the pollutant removal process more time-consuming (Hao et al. 2020; Chen et al. 2017). To overcome these limitations, various approaches were employed, including heat (Chen et al. 2017), light (Milh et al. 2021), metal materials (Xu et al. 2022a, b; Qin et al. 2020), carbon materials (Cai et al. 2021), and even a combination of the two methods (Giannakopoulos et al. 2022) to activate PS.

Biochar, with a large surface area and oxygen-containing functional groups (e.g., carboxyl, hydroxyl, and aromatic structures) can adsorb pollutants (Li et al. 2017a; b) and has been demonstrated to activate PS by radical-initiated process, such as ·OH (Leichtweis et al. 2020), $SO_4^{\cdot-}$. (Liang et al. 2020); Hao et al. 2020). Biochar further could accelerate electron transfer (Qu et al. 2024), or surface-bound free radicals (Liang et al. 2020) for PS activation to accelerate pollutant decomposition. Modified biochar arouses a lot of attention in sustainable agriculture, pollution remediation, and catalytic reactions (Panahi et al. 2020; Li et al. 2023; Shafizadeh et al. 2023).To increase the activation efficiency of biochar for PS, it was modified with metals (Han et al. 2015; Peiris et al. 2017; Liang et al. 2021). The metal loaded biochar and its degradation

of pollutants in published researches are listed in Additional file 1: Table S1 in support information. Fe-modified biochar had better tetracycline removal than non-modified biochar (Yang et al. 2016; Peiris et al. 2017). The participation of Fe improved the electron transfer capacity of biochar, resulted in more effective activation of PS and production of more $SO_4^{\cdot-}$ (Pan et al. 2022). The removal efficiency of chloraniline by a CuO/PS system could reach 71.5% within 5 h (Du et al. 2019), and that of oxytetracycline reached 75% in an Mn-modified biochar system (Fang et al. 2022). Due to the rich valence states, high reactivity, and low cost, Fe and Mn are always chosen to modify biochar for PS activation (Yang et al. 2019; Xu et al. 2023; Zhang et al. 2021a).

Compared to monometallic biochar composites, Fe–Mn bimetallic biochar composites were more effective in PS activation, and the removal efficiency of thiacloprid increased from 46.3–77.3% in monometallic biochar system to 94.1% after reaction for 90 min (He et al. 2022). The degradation efficiency of Orange G by PS activated with Fe–Mn bimetallic biochar (75.2%) was also higher than monometallic Fe-loaded biochar (45.6%) and Mn-loaded biochar (32.8%) (Hao et al. 2020). Although bimetallic biochar composites were proved to be more efficient in PS activation than monometallic ones, most previous studies focused on the performance differences in PS activation and the removal of organic contaminants, while the roles of Fe and Mn in this process remains unclear. These two metals in bimetallic biochar might have different effects on improving the oxidative degradation and adsorption of organic pollutants. Furthermore, there might exist a synergy between these two metals for the activation of PS. Therefore, the role of Fe and Mn in Fe–Mn bimetallic biochar on PS activation as well as the removal of organic pollutants should be further elucidated.

In this study, using atrazine as the target pollutant, Fe-rich and Mn-rich bimetallic biochar composites with similar total amounts of Fe and Mn were fabricated to activate PS for atrazine removal. Pristine biochar, Fe-based, and Mn-based monometallic biochar composites were investigated for comparison. The objectives of this research were: (1) to evaluate the decontamination efficiency of atrazine by monometallic and bimetallic biochar composites in PS systems; (2) to reveal the different roles of Fe and Mn on bimetallic biochar composites in the generation of reactive oxygen species as well as the atrazine decontamination; and (3) to elucidate the degradation pathway of atrazine in the bimetallic biochar composite/PS system. This study shed light on the fabrication of more effective bimetallic biochar composites for pollutant decontamination.

2 Materials and methods

2.1 Experimental reagents

Atrazine ($C_8H_{14}ClN_5$; 97%) was purchased from Shanghai Maclean Biochemical Technology Co., Ltd, Shanghai, China; Methanol (CH_3OH), ferrous sulfate heptahydrate ($FeSO_4{\cdot}7H_2O$), manganese chloride tetrahydrate ($MnCl_2{\cdot}4H_2O$), sodium persulfate ($Na_2S_2O_8$), sulfuric acid (H_2SO_4), hydrochloric acid (HCl), sodium hydroxide (NaOH), ethanol (C_2H_6O), and potassium bromide (KBr) were all of analytical purity and obtained from Sino Biopharmaceutical Chemical Reagents Co., LTD, Ningbo, China.

2.2 Preparation of biochar and modified biochar

To produce pristine biochar, the rice straw was washed, crushed, dried, and pyrolyzed at 500 °C for 3 h in a muffle furnace under an N_2 atmosphere. After cooling, the solid products were ground and passed through a 100-mesh sieve to obtain rice straw biochar, labeled as BC.

To produce Fe/Mn monometallic and bimetal biochar composites, different doses of $FeSO_4{\cdot}7H_2O$ and $MnCl_2{\cdot}4H_2O$ were dissolved in a specific amount of deionized water to achieve the Fe: Mn molar ratio of 3:1, 1:3, 2:0, and 0:2, respectively. Rice straw was then introduced into the prepared Fe–Mn binary or mono solutions. The solid–liquid ratio of rice straw to the solution was set at 1:10, and after impregnation for 12 h, the mixtures were filtered and dried in the oven at 85 °C. The subsequent steps were identical to the BC preparation. The Fe/Mn-loaded biochar obtained with Fe:Mn molar ratios of 3:1, 1:3, 2:0, and 0:2 was named as Fe-BBC, Mn-BBC, Fe-MBC, and Mn-MBC, respectively. The schematic of material synthesis is showed in Fig. 1.

2.3 The atrazine removal experiments

To assess the decontamination of atrazine and the activation of PS by biochar and modified biochar, atrazine removal experiments were conducted. All batch experiments were carried out in an oscillator (150 rpm, 25 °C) in the dark and performed in triplicate. In each experiment, 0.1 g of biochar (BC) or Fe/Mn modified biochar (Fe-BBC, Mn-BBC, Fe-MBC, and Mn-MBC) was added to 40 mL of atrazine solution with an initial concentration of 10 mg L^{-1} or a mixed solution containing 2 mM sodium persulfate and 10 mg L^{-1} atrazine, respectively. The pH was adjusted to 7 using NaOH and HCl (0.1 mol L^{-1}). Samples at 5, 10, 20, 30, 40, 60, 80, and 120 min were selected, and 1 mL sodium thiosulfate (0.5 mol L^{-1}) was added to terminate the oxidation reaction. The concentration of atrazine filtered by a membrane (0.22-μm) in the solution was detected. Since both adsorption and degradation contributed to the removal of atrazine in the

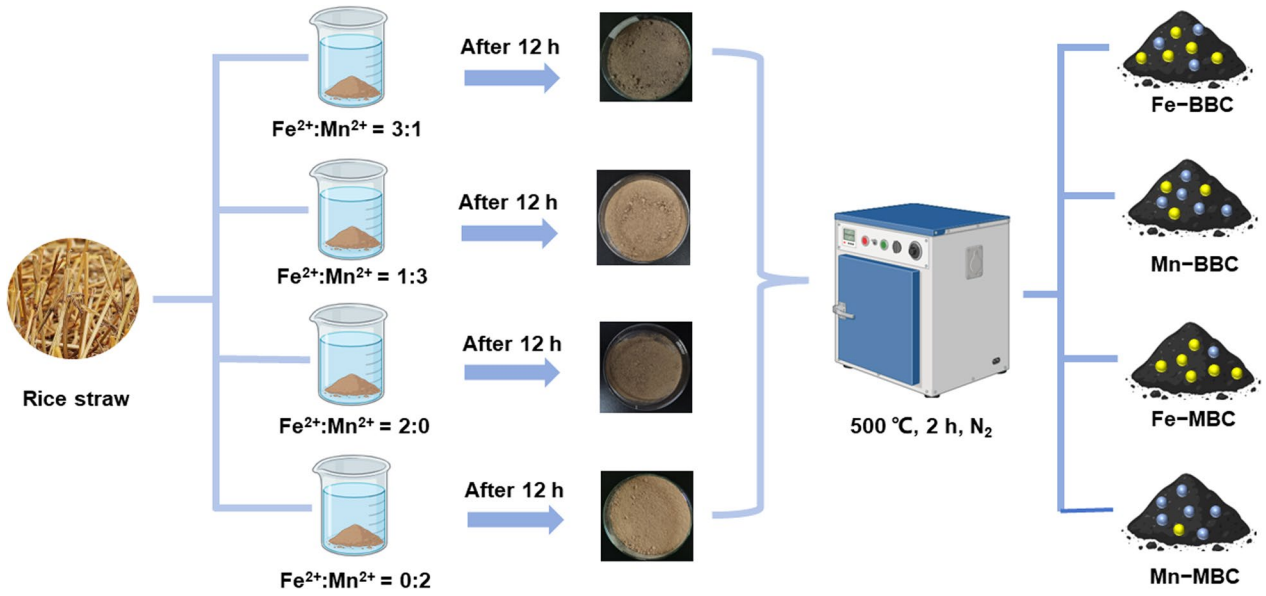

Fig. 1 The schematic of material synthesis

mixture solution. The filtered solids after a 120 min reaction were freeze-dried and extracted with 40 mL methanol through 6 h of shaking. This process aimed to detect any residual atrazine adsorbed on biochar or Fe/Mn-modified biochar. The calculation of the total removal amount (Q_T), the adsorption amount (Q_s), and the degradation amount (Q_d) of atrazine are shown in Additional file 1.

The filtered solids of Fe-BBC and Mn-BBC at 0, 30, and 120 min of reaction were subjected to XPS to investigate the valent change of Fe and Mn loaded on biochar in PS activation. The filtered solid in the Fe-BBC + PS system was employed to analyze reactive oxygen species using Electron Paramagnetic Resonance (EPR).

2.4 The quenching experiments

Quenching experiments were conducted to elucidate radicals and nonradicals involved in atrazine degradation in the biochar + PS and Fe/Mn-loaded biochar + PS systems. Ethanol (200 mM) and tert-Butanol (TBA, 200 mM) were carried out to distinguish ·OH and $SO_4^{\cdot-}$, respectively (Chen et al. 2020; Xu et al. 2022a, b). NaF (20 mM) served as the quencher for surface-bound radicals (Wang et al. 2022), and furfuryl alcohol (FFA, 0.4 mM) was introduced to identify the presence of $^1O_2$ (Fan et al. 2019). Samples were collected at 10, 30, 60, and 120 min, respectively, and promptly quenched by adding 100 μL of sodium thiosulfate (0.5 mol L^{-1}) to terminate the oxidation reaction. After filtration through a 0.22-μm membrane, the concentration of atrazine in the solution was detected. All samples were collected in triplicate.

2.5 The atrazine degradation pathways

To accurately reveal the atrazine degradation pathways, the degradation products and DFT calculations were examined, especially in the Fe-BBC + PS system with the highest degradation efficiency of atrazine. The solution in the Fe-BBC + PS system after 120 min of reaction was analyzed by high-performance liquid chromatography (HPLC–MS) to determine the degradation products. The atrazine degradation pathways were deduced by the degradation products.

Density functional theory (DFT) calculations were carried out using Gaussian 09 software, and the atrazine structure was optimized using the basis group of B3LYP/6-31G[d] and exported using Gauss View 5.0 software. The highest occupied molecular orbital (HOMO) and the lowest unoccupied molecular orbital (LOMO) were estimated by solvent (water) model using the self-consistent reactive field (SCRF)-based theory, which was used for the further study of the degradation pathways (An et al. 2023).

2.6 Analysis methods

The specific surface area, pore size, and pore volume of biochar were determined using Brunauer–Emmett–Teller (BET, Beijing Jinangpu V-sorb2800, China). Fourier transform infrared spectroscopy (FT-IR, Thermo Fisher Scientific NicoletIS5, USA) was employed to measure and analyze changes in surface functional groups before and after modification. The crystal structure of biochar was analyzed using an X-ray diffractometer (XRD, Bruker

D8, Germany). X-ray photoelectron spectroscopy (XPS, Thermo Fisher EscaL-ab 250Xi, USA) was used to analyze the binding energy of elements on the surface of biochar. An electron paramagnetic resonance spectrometer (EPR, Bruker EMXplus, Germany) was employed to measure and analyze the ·OH and $SO_4^{\cdot-}$ generated in the PS system.

The concentrations of Fe and Mn on biochar or modified biochar were determined using flame atomic absorption spectrometry (AAS, Agilent 3510, USA). The concentration of atrazine was analyzed by HPLC (LC-20AT, Japan). The degradation products were detected using LC–MS. A high-performance liquid chromatograph with Ultimate 3000 (Thermo Fisher Scientific, USA) and a resolution mass spectrometer 5600 QTOF (AB Sciex, Framingham, USA) was used. The detection conditions were the same as our previous research (Liang et al. 2022). After the reaction for 120 min, SPSS software was used to analyze the significance of the atrazine removal efficiency by various quenchers.

3 Results and discussion

3.1 Characterization of Fe/Mn monometallic and bimetallic biochars

The basic physicochemical property and amounts of Fe, Mn, or Fe + Mn loaded on biochar (BC), monometallic biochar (Fe-MBC, Mn-MBC), and bimetallic biochar (Fe-BBC, Mn-BBC) are shown in Table 1. Compared with BC, the modified biochar exhibited significantly higher Fe and Mn content. It showed higher total Fe and Mn amounts in bimetallic biochar (0.946 mol kg^{-1} on Mn-BBC and 0.998 mol kg^{-1} on Fe-BBC) than in monometallic biochar (0.765 mol kg^{-1} on Mn-MBC and 0.781 mol kg^{-1} on Fe-MBC). However, the total metal amount was similar between Fe-loaded biochar and Mn-loaded biochar, 0.947 vs 0.998 mol kg^{-1} for bimetallic biochar, and 0.781 vs 0.765 mol kg^{-1} for monometallic biochar. The loading of Fe or Mn on the surface of biochar had different effects on the basic physicochemical properties of biochar. As shown in Table 1, the specific surface area (SSA) of Fe-BBC and Fe-MBC were 148 and 54.4 $m^2\ g^{-1}$, respectively, which were 17.2 and 6.31 times compared to pristine biochar (8.61 $m^2\ g^{-1}$). However, the SSAs of Mn-BBC and Mn-MBC were 4.00 and 5.04 $m^2\ g^{-1}$, respectively, significantly lower than that of pristine biochar. The larger SSAs of Fe-BBC and Fe-MBC could be attributed to the catalytic cracking of oxygen complexes by the loaded Fe (Zhang et al. 2021a; Yang et al. 2018). Compared with pristine biochar, the pore size of Mn-BBC and Mn-MBC increased by 3.04 times and 2.38 times, respectively, indicating that Mn played a key role in micropore creation (Li et al. 2017a, b). The larger pore sizes facilitated the entry of pollutants into the adsorption sites (Li et al. 2017a, b), thereby increasing the adsorption capacity of biochar. These findings suggest that Fe and Mn were involved in the formation of biochar pore structure during pyrolysis, and were successfully loaded on the biochar surface. The Fe and Mn loaded on biochar also increase the pHpzc.

The higher metallic oxides on the biochar surface could provide more adsorption sites and form complexes with pollutants (Zhang et al. 2021a). FTIR spectra of biochar and modified biochar (Additional file 1: Fig. S1a) revealed the presence of the Fe–O bond on the carbon ring (558 cm^{-1}) in Fe-based monometallic biochar (Fe-MBC), the Mn–O (776 cm^{-1}) bond in Mn-based monometallic biochar (Mn-MBC), as well as Mn–O and Fe–O bond in Mn-rich bimetallic biochar (Mn-BBC) and Fe-rich bimetallic biochar (Fe-BBC). These results also suggest the successful loading of Fe/Mn on biochar, which might predominantly exist in the form of metal oxides. XRD patterns of the different modified biochar in the range of 20°–65° (Additional file 1: Fig. S1b) further showed that the Mn_3O_4 was present in Mn-MBC, Fe_3O_4 in Fe-MBC, Mn_3O_4 and $FeMnO_3$ in Mn-BBC as well as Fe_3O_4 and $FeMnO_3$ in Fe-BBC. The ratio of Fe and Mn added to the feedstock significantly influenced the types of metal oxides formed during the pyrolysis of both monometallic and bimetallic biochar. The distinct characteristics of Fe/

Table 1 Specific surface area, pH, Fe, and Mn in biochar and Fe/Mn loaded biochar

Material	Specific surface area	Average pore size	Pore volume	pH_{pzc}	Fe	Mn	Fe + Mn
	$m^2\ g^{-1}$	nm	$cm^3\ g^{-1}$		mol kg^{-1}		
BC	8.61	7.70	0.017	2.20	0.178	0.029	0.207
Fe-MBC	54.4	5.53	0.075	2.56	0.767	0.014	0.781
Mn-MBC	5.04	18.4	0.037	2.76	0.315	0.450	0.765
Mn-BBC	4.00	23.4	0.043	2.63	0.443	0.504	0.947
Fe-BBC	148	4.28	0.159	2.58	0.772	0.226	0.998

Mn monometallic and bimetallic biochar might significantly impact their adsorption and the activated PS degradation of atrazine.

3.2 Removal of atrazine in different systems

Figure 2 illustrates the removal of atrazine in biochar, PS, and biochar + PS systems. The atrazine concentration in the solution decreased with reaction time in all systems (Fig. 2a, Additional file 1: Fig. S2). After reaction for 120 min, the total amount of atrazine removed was 626.7 mg kg^{-1} for BC, 1000 mg kg^{-1} for Fe-MBC, 1133 mg kg^{-1} for Mn-MBC, 1653 mg kg^{-1} for Fe-BBC, and 1360 mg kg^{-1} for Mn-BBC, respectively. Correspondingly, the removal rates of atrazine were 15.7% for pristine biochar, and higher for modified biochar, reaching 25.0%, 28.3%, 34.0%, and 41.3% for Fe-MBC, Mn-MBC, Mn-BBC, and Fe-BBC, respectively (Fig. 2b). The atrazine removal occurred primarily through adsorption for both pristine and modified biochar, while degradation made a limited contribution (≤2.3%, Fig. 3a). Bimetallic biochar demonstrated a greater adsorption capacity for atrazine than monometallic biochar. The total amounts of Fe and Mn in bimetallic biochar, Mn-BBC (0.946 mol kg^{-1}) and Fe-BBC (0.998 mol kg^{-1}) were significantly higher than those on monometallic biochar, Fe-MBC (0.781 mol kg^{-1}) and Mn-MBC (0.765 mol kg^{-1}) (Table 1). The higher metal oxides on the biochar surface could provide more adsorption sites and form complexes with pollutants (Zhang et al. 2021a).

The PS alone exhibited very low removal efficiency of atrazine (7.67%) after the reaction for 120 min, indicating the limited decomposition of PS without the addition of an activator (Luo et al. 2022). However, the decontamination efficiency of atrazine was significantly improved when biochar was introduced into the PS system. After the reaction for 120 min, the removal efficiency of atrazine in the BC + PS system increased to 22.7%, 1.45 times higher than that of BC alone. The modified biochar + PS systems exhibited superior atrazine decontamination, achieving removal rates of 72.3% for Fe-MBC + PS, 61.3% for Mn-MBC + PS, 96.7% for Fe-BBC + PS, and 77.2% for Mn-BBC + PS, which were 2.89, 2.17, 2.27, and 2.30 times higher than Fe-MBC, Mn-MBC, Fe-BBC, and Mn-BBC, respectively. Fe-BBC showed a higher removal efficiency of atrazine (96.7%) than previously published research (Jiang et al. 2020; Zhang et al. 2021a, b), in which atrazine removal rates were 83.77% (Jiang et al. 2020) and 93.8% (Zhang et al. 2021a, b) in biochar-supported zero-valent iron + PS system, respectively.

These findings highlight that Fe and/or Mn on biochar played an important role in activating PS for atrazine decontamination or improving atrazine adsorption, and bimetallic biochar was more effective than monometallic biochar for atrazine decontamination in PS systems.

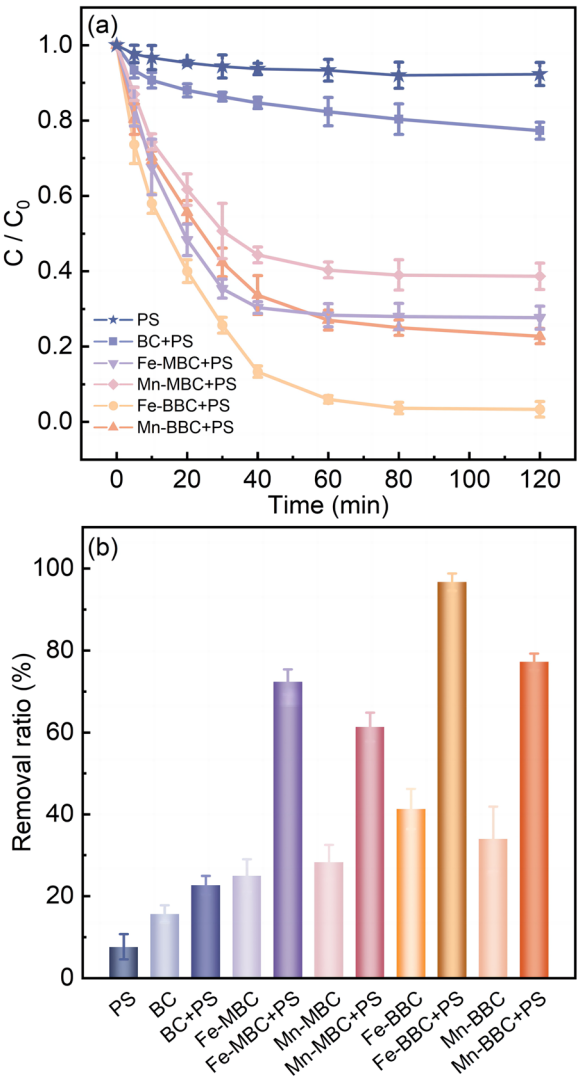

Fig. 2 **a** The atrazine concentration in the solution. **b** Total removal ratio of atrazine in different systems. $[ATZ]_0 = 10$ mg L^{-1}; $[BC]_0 = 0.1$ g; $[PS]_0 = 2$ mM; pH = 7; T = 25℃

Both adsorption and degradation contributed to the removal of atrazine in different PS systems. As shown in Fig. 3b, in the BC + PS system, 71.0% of atrazine removal was attributed to adsorption, while the remaining 29.0% was due to degradation. The ability of biochar for PS activation is closely related to its oxygen-containing functional groups, which could serve as electron donors or electron transfer mediators (He et al. 2022; Li et al. 2023). However, the atrazine degradation ratios significantly increased in the presence of modified biochar, constituting 59.8%, 56.2%, 65.6%, and 54.0% of atrazine removal in the systems of Fe-BBC + PS, Mn-BBC + PS, Fe-MBC + PS,

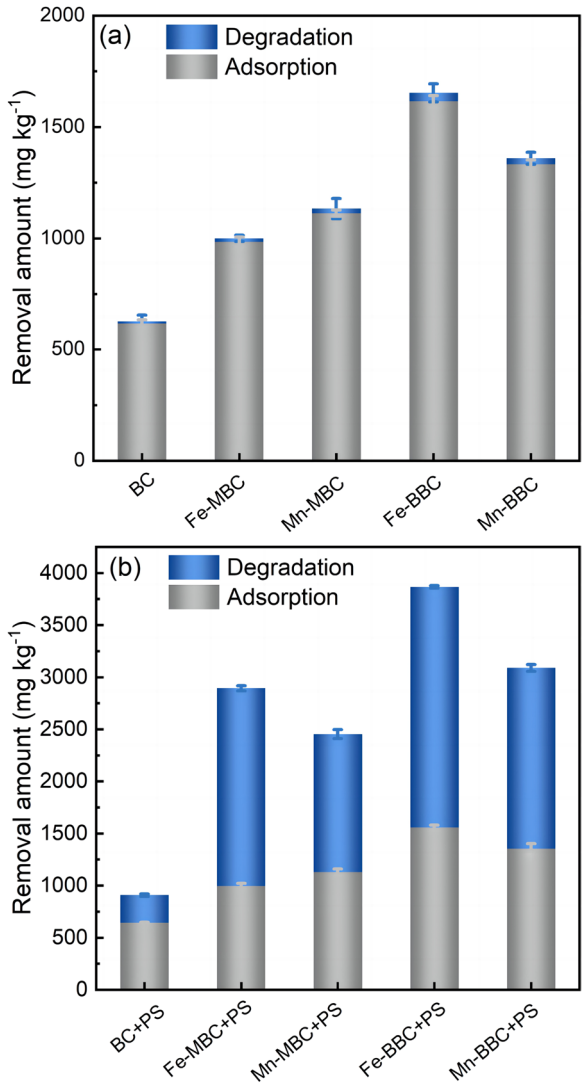

Fig. 3 **a** Contribution ratio of adsorption and degradation in biochar alone. **b** Biochar + PS system

and Mn-MBC + PS, respectively. The degradation rate of atrazine in modified biochar systems exceeded the adsorption rate, whereas adsorption dominated the atrazine removal in the BC system, suggesting that the activation of PS by metallic elements on the surface of biochar might be more effective than that by the oxygen-containing functional groups. Metals loaded on biochar, e.g. Fe, Mn, Cu, may enhance the electron transfer (Hao et al. 2020), provide more active sites for PS activation (Chen et al. 2020), and then accelerate catalytic reactivity. The correlation between the atrazine adsorption of biochar and the atrazine degradation in the biochar + PS system is shown in Additional file 1: Fig. S3. The Pearson correlation coefficient for adsorption and degradation was 0.899, signifying a favorable relationship between adsorption and degradation. The synergy between adsorption and degradation might contribute to the higher removal efficiency of atrazine in bimetallic biochar systems, compared to monometallic biochar systems.

In addition, higher degradation rates were observed in Fe-rich biochar (Fe-BBC and Fe-MBC) than in Mn-rich biochar (Mn-BBC and Mn-MBC) (Fig. 3b), indicating that the activation of PS by Fe-rich biochar was more favorable than that of Mn-rich biochar, resulting in higher atrazine degradation amount of 1914–2385 mg kg^{-1}, compared to 1321–1746 mg kg^{-1}. The Fe/Mn efficiency for atrazine degradation (mol/mol) was 1.07×10^{-2} for Fe-BBC + PS, 0.85×10^{-2} for Mn-BBC + PS, 1.13×10^{-2} for Fe-MBC + PS, and 0.80×10^{-2} for Mn-MBC + PS, respectively, followed by Fe-MBC > Fe-BBC > Mn-BBC > Mn-MBC. This result further confirmed that Fe was more favorable for atrazine degradation than Mn in PS systems. Detailed explanations are presented in Sects. 3.3 and 3.4.

3.3 Roles of Fe and Mn loaded on biochar in free radicals and nonradicals generation

To further investigate the different roles of Fe and Mn loaded on biochar for PS activation, chemical quenching tests using tert-butanol (TBA), methanol (MeOH) NaF, and furfuryl alcohol (FFA) were conducted. MeOH can rapidly react with $SO_4^{\cdot-}$ and ·OH in the solution (Chen et al. 2020). The reaction rate of TBA with ·OH in the solution (6×10^8 M^{-1} s^{-1}) is significantly higher than that of $SO_4^{\cdot-}$ (4×10^5 M^{-1} s^{-1}), indicating that TBA is primarily responsible for consuming ·OH (Xu et al. 2022a, b). FFA was introduced into the system to detect $^1O_2$, and their reaction exhibited a second-order rate constant of 1.2×10^8 M^{-1} s^{-1} (Jiang et al. 2017). NaF served as the quencher for surface-bound radicals. Figure 4a shows that the addition of MeOH (200 mM) inhibited 1.15% of atrazine removal in BC + PS, while there was a negligible reduction of atrazine when adding TBA (200 mM), NaF (20 mM), and FFA (0.4 mM). These results suggested that ·OH was responsible for the limited atrazine degradation in the BC + PS system.

In the Fe-rich biochar + PS system, the addition of TBA resulted in a reduction of atrazine removal by 8.8% and 4.7% for Fe-BBC and Fe-MBC, respectively. Similarly, the addition of MeOH decreased the removal of atrazine by up to 12.2% and 9.2% for Fe-BBC and Fe-MBC, respectively. This observation indicated that $SO_4^{\cdot-}$ and OH contributed to the oxidative degradation of atrazine in the Fe-rich biochar + PS system (Eqs. 1–2). EPR tests using DMPO as the trapping agent for the Fe-BBC + PS system resulting in four-line spectra of the adduct DMPO-OH with a relative strength ratio of 1:2:2:1 and the adduct DMPO-$SO_4^{\cdot-}$ with a relative

strength ratio of 1:1:1:1:1 (Qu et al. 2023) (Fig. 4f), confirming the presence of $SO_4^{\cdot-}$ and ·OH in the Fe-BBC + PS system. The addition of FFA and NaF barely affected the removal of atrazine in both Fe-MBC + PS and Fe-BBC + PS systems, proving that surface-bound radicals and $^1O_2$ did not contribute to the degradation of atrazine. These results suggested atrazine degradation in Fe-rich biochar systems was mainly attributed to free radicals (i.e., $SO_4^{\cdot-}$ and ·OH). However, $^1O_2$ contributed to the degradation of atrazine in the Mn-MBC + PS system, evidenced by a 12.2% inhibition of atrazine degradation upon FFA addition. The presence of Mn(II) or Mn(III) facilitated the reaction with PS in the solution to generate $O_2^{\cdot-}$, which further produced $^1O_2$ through Eq. (3–4). Qu et al. (2024) also found $^1O_2$ could be produced by reaction between C=O on biochar and PS and transformation of $O_2^{\cdot}$ and ·OH. $SO_4^{\cdot-}$ also contributed to atrazine degradation in the Mn-MBC + PS system (Eqs. 5–6), as indicated by a 6.4% inhibition of atrazine degradation with the addition of MeOH and negligible inhibition by the addition of TBA and NaF. In the Mn-BBC + PS system, the addition of MeOH, NaF, TBA, and FFA resulted in decreases in atrazine degradation by 6.7%, 6.2%, 4.1%, and 3.4%, respectively. These results suggested that both free radicals and non-free radicals played a crucial role in the degradation of atrazine in this system.

$$Fe^{2+} + S_2O_8^{2-} \rightarrow Fe^{3+} + SO_4^{2-} + SO_4^{\cdot-}. \quad (1)$$

$$SO_4^{\cdot-} + OH^- \rightarrow \cdot OH + SO_4^{2-}. \quad (2)$$

$$O_2^{\cdot-} + \cdot OH \rightarrow {}^1O_2 + OH^-. \quad (3)$$

$$2O_2^{\cdot-} + H_2O \rightarrow H_2O_2 + {}^1O_2 + 2OH^-. \quad (4)$$

$$Mn^{3+} + S_2O_8^{2-} \rightarrow Mn^{4+} + SO_4^{2-} + SO_4^{\cdot-}. \quad (5)$$

$$Mn^{2+} + S_2O_8^{2-} \rightarrow Mn^{3+} + SO_4^{2-} + SO_4^{\cdot-}. \quad (6)$$

In summary, the atrazine degradation in Fe-rich biochar systems was mainly attributed to free radicals, $SO_4^{\cdot-}$ and ·OH, while both radical and non-radical species existed in Mn-rich biochar systems. Compared to non-radical species, $^1O_2$ and surface-bound radicals, the oxidation potential of free radicals was much higher, and more atrazine was degraded in Fe-rich biochar (Fe-BBC and Fe-MBC) systems than in Mn-rich biochar (Mn-BBC and Mn-MBC) systems.

3.4 Mechanisms of Fe and Mn loaded on biochar in the PS activation

The bimetallic biochar demonstrated superior performance for atrazine removal in PS systems compared to monometallic biochar, which was attributed to the synergy of adsorption and degradation, stemming from a higher concentration of metal oxides. Interestingly, when comparing Mn-BBC and Fe-BBC, even with a similar total amount of Fe/Mn (0.994 vs 0.947 mol kg^{-1}), their performances for atrazine degradation in PS systems differed significantly, suggesting the ratio of Fe and Mn had a significant effect on atrazine degradation. Consequently, further analysis of Fe-BBC and Mn-BBC during the reaction was conducted to elucidate the specific contributions of Fe and Mn in PS activation for atrazine degradation.

To identify the variation of valence states of Fe and Mn, XPS analysis was performed on Fe-BBC and Mn-BBC at 0, 30, and 120 min, and is depicted in Figs. 5 and 6. The binding energies of Fe(II) were presented on 711 eV at $Fe2p_{3/2}$ and 724.6 eV at Fe $2p_{1/2}$, while those of Fe(III) were presented on 714.5 at $Fe2p_{3/2}$ and 728.1 eV at Fe $2p_{1/2}$. The Mn peak at Mn $2p_{3/2}$ can be divided into three peaks corresponding to Mn (II) (641.0 eV), Mn(III) (642.6 eV), and Mn(IV)(643.8 eV). Prior to the reaction, higher percentages of Fe(II), Mn(II), and Mn(III) were observed on the surface of Fe-BBC, with values of 71.8%, 51.4%, and 40.5%, respectively, while those of Mn-BBC were 68.9%, 52.3%, and 37.6%, respectively (Table 1, Figs. 5a, 6a). These results indicated that the ratio of Fe and Mn added to the feedstock had great influence on the types of metal oxides during the generation of bimetallic biochar. With higher Fe(II), Mn(II), and Mn(III), Fe-BBC could supply more electrons to PS than Mn-BBC, which might be responsible for the better degradation of atrazine in the Fe-BBC + BC system. With an increase in the reaction time from 0 to 120 min, in the Mn-BBC + PS system, the percentages of Fe(II) and Mn(II) decreased from 68.9% to 60.8%, and from 52.3% to 37.0%, respectively. Concurrently, the percentages of Fe (III), Mn(III), and Mn(IV) increased from 31.1% to 39.2%, 37.6% to 44.5%, and 10.1% to 18.5%, respectively (Figs. 5, 6). The continuous decrease in Fe(II) and Mn(II) was primarily attributed to their reactions with PS, leading to the formation of $SO_4^{\cdot-}$ (Eqs. 1, and 5–6), and $^1O_2$ (Eqs. 3–4) as mentioned in Sect. 3.3. XPS O1s spectra analysis of Mn-BBC + PS system revealed that the M–O bond at 530.89–531.16 eV was up to 60.1% at 30 min and decreased to 41.6% at 120 min (Additional file 1: Fig S4a–c), implying that surface-bound radical and adsorption by metal oxide also contributed to the reduction of atrazine, consistent with the results mentioned above.

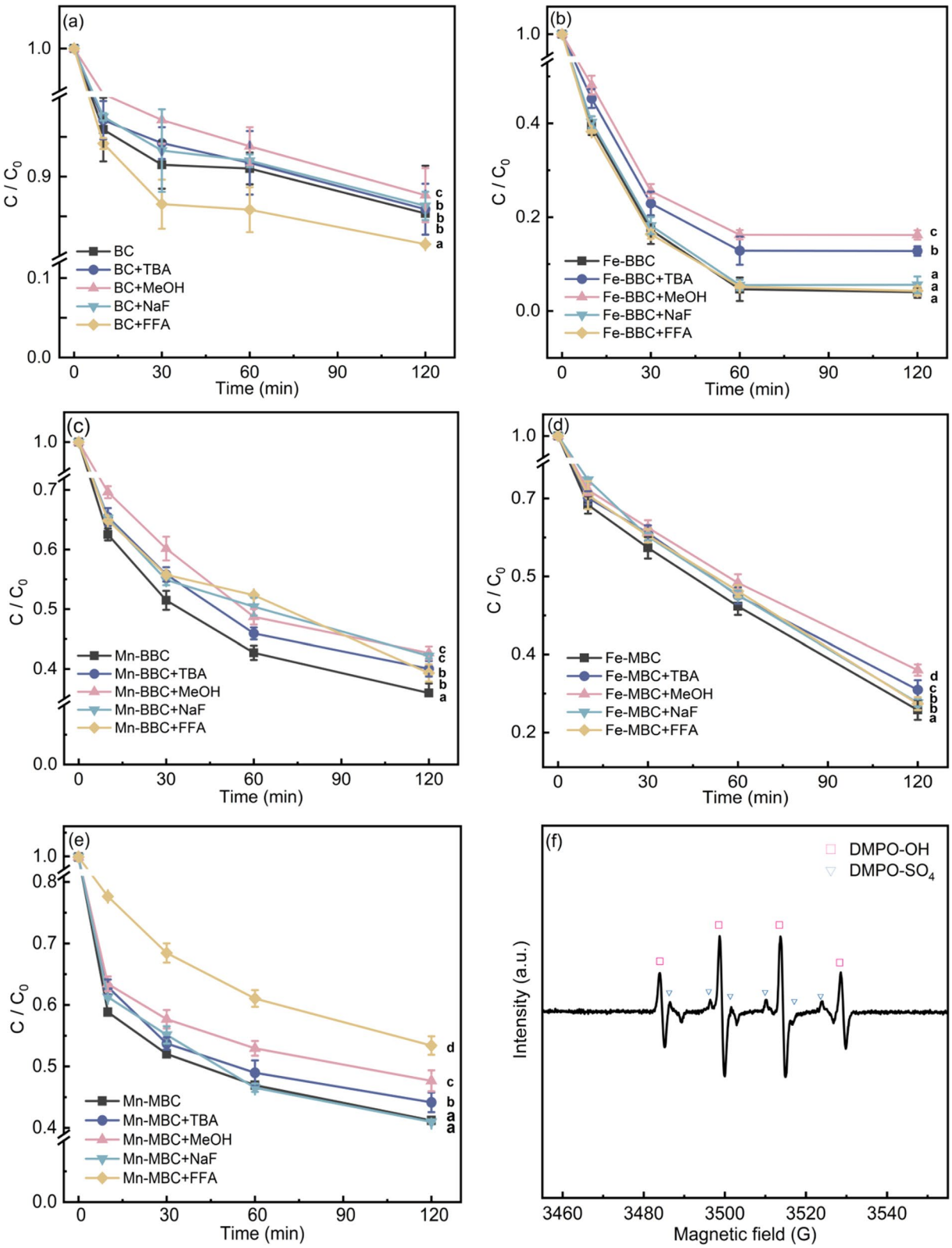

Fig. 4 Effects of radical and nonradical contribution on atrazine removal in (**a**) BC, (**b**) Fe-BBC, (**c**) Mn-BBC, (**d**) Fe-MBC, and (**d**) Mn-MBC $[ATZ]_0 = 10$ mg L^{-1}; $[BC]_0 = 0.1$ g; $[PS]_0 = 2$ mM; pH = 7; T = 25 ℃; [TBA/MeOH] = 200 mM (**f**) EPR profile of Fe-BBC + PDS system

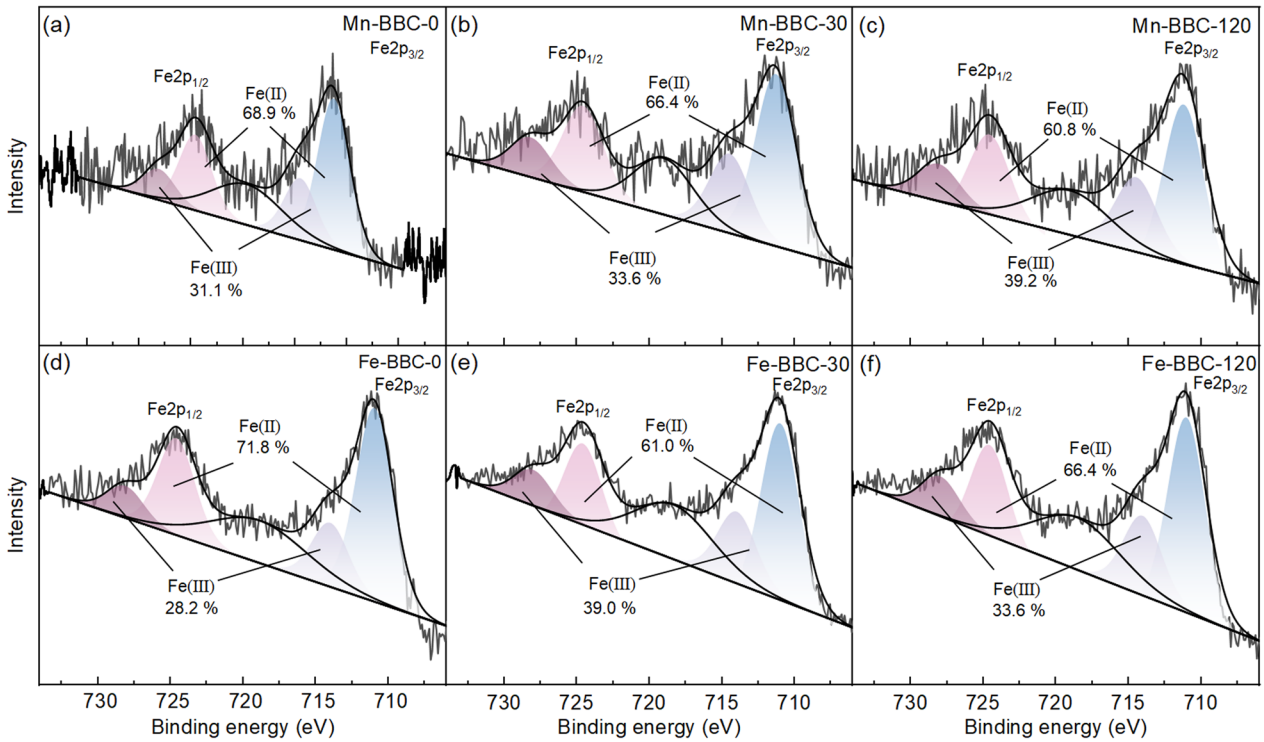

Fig. 5 The fine XPS spectra of Fe on Mn-BBC (**a**)–(**c**) and Fe-BBC (**d**)–(**f**) at the reaction time of 0, 30, and 120 min

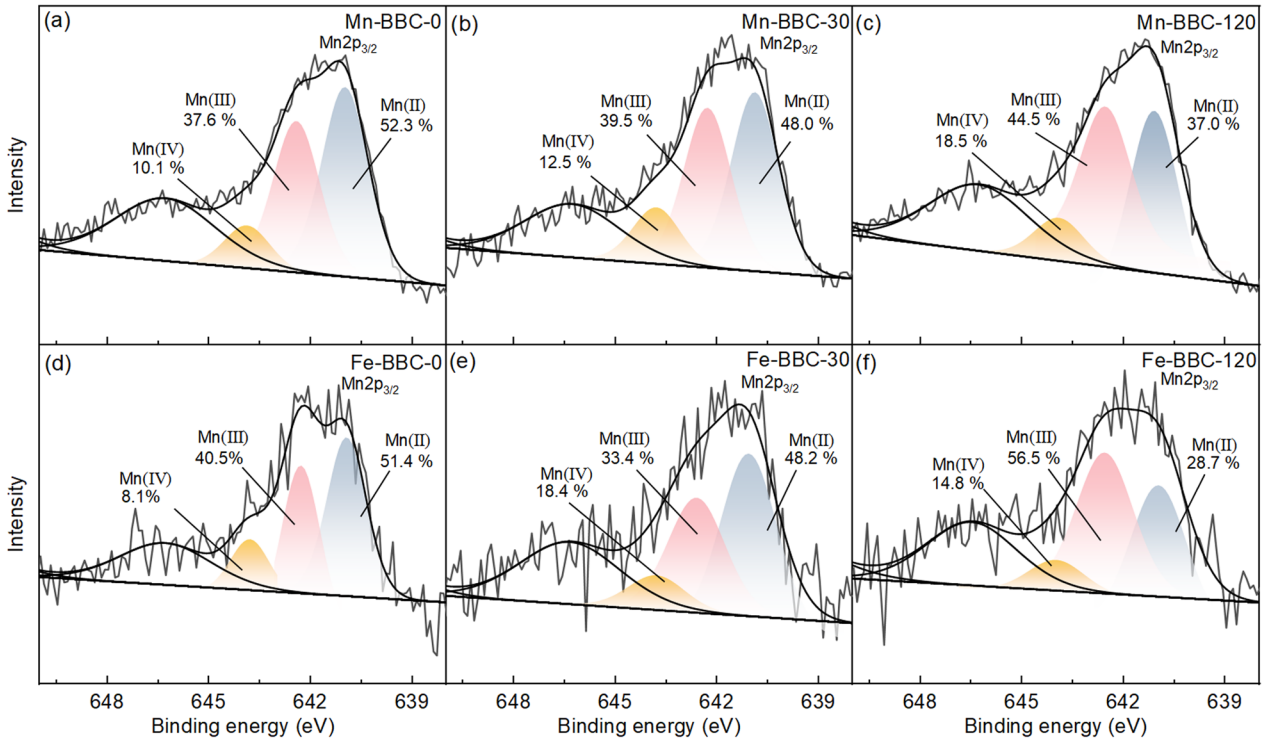

Fig. 6 The fine XPS spectra of Mn on Mn-BBC (**a**)–(**c**) and Fe-BBC (**d**)–(**f**) at the reaction time of 0, 30, and 120 min

Unlike Mn-BBC with the continuous decrease of Fe(II) and Mn(II) as well as the continuous increase of Fe(III), Mn(III), and Mn(IV) during the whole reaction time, for Fe-BBC, the ratio of Fe(II) and Mn(III) decreased at 30 min and then increased at 120 min, while the ratio of Fe(III) and Mn(IV) increased at 30 min and then decreased at 120 min. The fluctuations in the metal valence state on Fe-BBC suggested the possible electron exchange between Fe and Mn species. The redox potentials of Mn(IV)/Mn(III), Mn(III)/Mn(II), and Fe(III)/Fe(II) were 0.51, 1.51, and 0.77 V, respectively (Hao et al. 2020), so Mn(III) or Mn(IV) should react with Fe(II) or Fe(III), according the Eqs. (7–9) (Cai et al. 2021). With the higher radio of Mn(III) in the Fe-BBC + PS system,

Table 2 Molecular formula, structural formula, mass-to-charge ratio, retention time and abbreviation of atrazine and its intermediates

Molecular formula	Structural formula	Mass-to-charge ratio (m/z)	Retention time (min)	Abbreviation
$C_8H_{14}ClN_5$	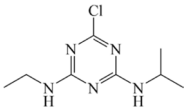	216.10	1.65	ATZ
$C_6H_8ClN_5O_2$	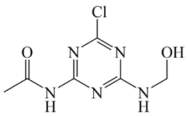	217.01	2.4	CNDT
$C_6H_{10}ClN_5$	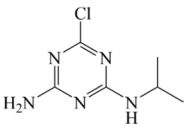	188.07	6.95	CAIT
$C_5H_8ClN_5$	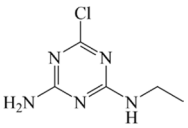	174.05	5.84	DIA
$C_5H_6ClN_5O$	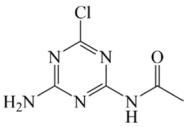	188.03	2.68	CADT
$C_3H_4ClN_5$	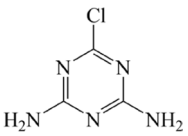	146.02	1.62	CAAT
$C_8H_{15}N_5O$	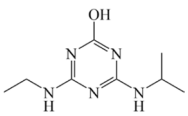	198.12	605	OEIT
$C_8H_{13}N_5O_2$	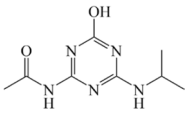	212.10	3.03	ODIT
$C_6H_{11}N_5O$	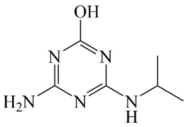	170.1	1.04	OAIT
$C_5H_7N_5O_2$	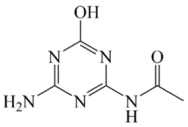	170.06	1.49	OEAT

the conversion of Fe(II) from Fe(III) by Mn(III) was favorable on the surface of Fe-BBC. The valence state exchange between Fe and Mn might contribute to the continuous and robust decomposition of PS and the significant degradation of atrazine.

$$Mn^{3+} + Fe^{2+} \rightarrow Mn^{2+} + Fe^{3+}. \quad (7)$$

$$Mn^{3+} + Fe^{3+} \rightarrow Mn^{4+} + Fe^{2+}. \quad (8)$$

$$Mn^{4+} + Fe^{2+} \rightarrow Mn^{3+} + Fe^{3+}. \quad (9)$$

3.5 Degradation pathways of atrazine

Based on previous studies, the potential pathways for atrazine degradation involved alkyl hydroxylation, alkyl oxidation, dealkylation, and the four processes of dichlorination and hydroxylation (Jiang et al. 2020; Tian et al. 2021; Wu et al. 2018; Zhang et al. 2021b). To further reveal the atrazine degradation pathways in the Fe-BBC + PS system, the degradation products were detected and DFT calculations were performed. Table 2 shows nine atrazine degradation products, namely CNDT ($C_6H_8ClN_5O_2$), CAIT($C_5H_8ClN_5$), DIA($C_5H_8ClN_5$), CADT($C_5H_6ClN_5O$), CATT($C_3H_4ClN_5$), OEIT($C_8H_{15}N_5O$), ODIT($C_8H_{13}N_5O_2$), OAIT ($C_6H_{11}N_5O$), and OEAT($C_5H_7N_5O_2$). Based on the detection of these degradation products and the above-mentioned previous studies, three possible atrazine degradation pathways in the Fe-BBC + PS system were proposed (Fig. 7a).

In pathway 1, $SO_4^{\cdot-}$ and ·OH attacked the C–C and C–H bonds in the side chain of atrazine, leading to the formation of CNDT through alkyl hydroxylation and alkyl oxidation. Subsequently, one of the side chains of CNDT was attacked by free radicals, resulting in dealkylate to form CADT. This process continued with the breaking of the C–N bond, leading to the formation of CAAT. Finally, CAAT underwent dichlorination and hydroxylation by reacting with ·OH to yield the potential product OAAT.

In pathway 2, one of side chains of atrazine was initially attacked by $SO_4^{\cdot-}$ and ·OH, leading to the breaking of the C–N bond and the formation of the dealkylation product CAIT. This process continued with a similar dealkylation mechanism to produce DIA. Subsequently, one of the alkyl groups in DIA was oxidized by free radicals, resulting in the generation of CADT, and the subsequent degradation pathway followed the same step as in pathway1.

In pathway 3, ·OH initially reacted with atrazine, leading to dichlorination and hydroxylation and the production of OEIT. Subsequently, the C–C and C–H bonds in the side chain of OEIT were attacked by $SO_4^{\cdot-}$ and OH, resulting in alkyl hydroxylation and alkyl oxidation, to generate ODIT. Successive dealkylation and alkyl oxidation then occurred to form OAIT and OEAT. Subsequently, OEAT underwent dealkylation to produce OAAT, and the side chain of OAAT was oxidized by ·OH to form the less toxic cyanuric acid. It was reported that OAAT was the final product from the oxidative degradation of atrazine due to its strong resistance to radicals and the difficulty in its further degradation (Zhang et al. 2021b).

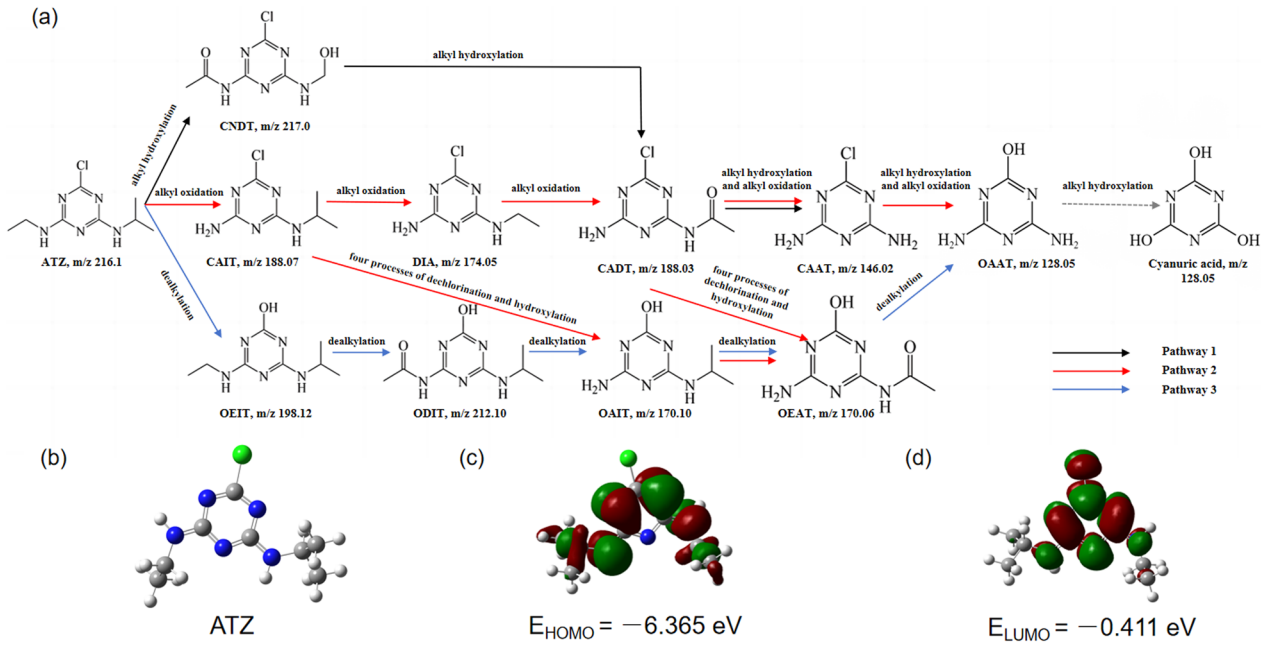

Fig.7 The possible atrazine degradation pathways in (**a**) Fe-BBC + PS system, (**b**) structure of atrazine, (**c**) HOMO, and (**d**)LUMO calculated by DFT

The structure of atrazine optimized by B3LYP/6-31G(d)] method is shown in Fig. 7b. The HOMO and LUMO of atrazine are shown in Fig. 7c, d, whose energy levels are −6.365 eV and −0.411 eV, respectively. The HOMO was located on the bilateral side chain of atrazine (Fig. 7c), consistent with the existence of the degradation pathways 1 and 2, where the bilateral side chain of atrazine was attacked by free radicals, such as $SO_4^{\cdot-}$ and ·OH (An et al. 2023; Zhang et al. 2021b). The LUMO was mainly distributed on the triazine ring and Cl atoms (Fig. 7d), consistent with the existence of the degradation pathway 3, where the production of OEIT was due to the attack of the C–Cl bond by ·OH.

4 Conclusions and prospects

In this study, Fe-rich and Mn-rich bimetallic biochar composites were prepared and the roles of Fe and Mn components for removal of PS-based atrazine were investigated. Although both bimetallic biochar composites could effectively remove atrazine, Fe-rich bimetallic biochar was more conducive to oxidative degradation. Atrazine degradation by Fe-rich monometallic and bimetallic biochar systems was mainly attributed to free radicals (i.e., $SO_4^{\cdot-}$ and ·OH), while both surface-bound radicals, $^1O_2$, and free radicals were responsible for the degradation of atrazine in Mn-rich biochar systems. Furthermore, with higher ratios of Fe(II) and Mn(III) formed in Fe-rich bimetallic biochar, the valence state exchange between Fe and Mn contributed to the more effective activation of PS and the generation of more free radicals. The atrazine degradation pathways in the Fe-rich bimetallic biochar systems involved alkyl hydroxylation, alkyl oxidation, dealkylation, and dechlorohydroxylation, which were established from the degradation products and DFT calculations. The results indicate that bimetallic biochar composites with more Fe and less Mn were more effective for the PS-based degradation of atrazine, which guided the development of carbon materials especial for modified biochar with active metals to renovate different kinds of pesticide polluted wastewater or soils.

Supplementary Information

The online version contains supplementary material available at https://doi.org/10.1007/s42773-024-00331-4.

Additional file 1: Table S1. The metal loaded biochar and its degradation of pollutants. **Table S2.** Abbreviations and symbols. **Figure S1.** FTIR patterns (a) and XRD patterns (b) of pristine biochar (BC), monometallic (Fe-MBC, Mn-MBC) and bimetallic biochar (Fe-BBC, Mn-BBC). **Figure S2.** The atrazine concentration in the solution in BC, Fe-BBC, Mn-BBC, Fe-MBC, and Mn-MBC. **Figure S3.** The correlation between the adsorption of atrazine in biochar alone and the degradation of atrazine in biochar+PS system. **Figure S4.** The fine XPS O1s spectra of Mn-BBC (a, b, c) and Fe-BBC (d, e, f) at 0, 30, and 120 min.

Acknowledgements
This work was supported by the National Natural Science Foundation of China (No. 21507097, No. 42207479, No. 22278419), 2022 Gusu Native Talent Program, and Suzhou key technology research (social development) project (2023SS06).

Author contributions
TR and ZB performed the experiment; LY, FY, and CYY contributed significantly to analysis and manuscript preparation; YL, KLZ, and ZB performed the data analyses and wrote the manuscript; MZD drew the graphical abstract. LHH performed the DFT calculation and analysis. All authors read and approved the final manuscript.

Availability of data and materials
Data will be shared upon reasonable request.

Declarations

Competing interests
The authors do not have any competing interests.

Author details
[1]School of Environmental Science and Engineering, Suzhou University of Science and Technology, Suzhou 215000, China. [2]School of Chemistry and Life Sciences, Suzhou University of Science and Technology, Suzhou 215000, China. [3]School of Environment and Architecture, University of Shanghai for Science and Technology, Shanghai 200093, China.

Received: 20 January 2024 Revised: 15 March 2024 Accepted: 30 March 2024
Published online: 22 April 2024

References

An Y, Li X, Liu Z, Li Y, Zhou Z, Liu X (2023) Constant oxidation of atrazine in Fe(III)/PDS system by enhancing Fe(III)/Fe(II) cycle with quinones: reaction mechanism, degradation pathway and DFT calculation. Chemosphere 317:137883. https://doi.org/10.1016/j.chemosphere.2023.137883

Asghar A, Abdul Raman AA, Wan Daud WMA (2015) Advanced oxidation processes for in-situ production of hydrogen peroxide/hydroxyl radical for textile wastewater treatment: a review. J Cleaner Prod 87:826–838. https://doi.org/10.1016/j.jclepro.2014.09.010

Bessac F, Hoyau S (2013) Pesticide interaction with environmentally important cations: a theoretical study of atrazine in interaction with two Ca^{2+} cations. Comput Theor Chem 1022:6–13. https://doi.org/10.1016/j.comptc.2013.06.025

Bohn T, Cocco E, Gourdol L, Guignard C, Hoffmann L (2011) Determination of atrazine and degradation products in Luxembourgish drinking water: origin and fate of potential endocrine-disrupting pesticides. Food Addit Contam Part A Chem Anal Control Exposure Risk Assess 28:1041–1054. https://doi.org/10.1080/19440049.2011.580012

Cai M, Zhang Y, Dong C, Wu W, Wang Q, Song Z, Shi Y, Wu L, Jin M, Dionysiou DD, Wei Z (2021) Manganese doped iron-carbon composite for synergistic persulfate activation: Reactivity, stability, and mechanism. J Hazard Mater 405:124228. https://doi.org/10.1016/j.jhazmat.2020.124228

Chen Y, Deng P, Xie P, Shang R, Wang Z, Wang S (2017) Heat-activated persulfate oxidation of methyl- and ethyl-parabens: effect, kinetics, and mechanism. Chemosphere 168:1628–1636. https://doi.org/10.1016/j.chemosphere.2016.11.143

Chen L, Jiang X, Xie R, Zhang Y, Jin Y, Jiang W (2020) A novel porous biochar-supported Fe-Mn composite as a persulfate activator for the removal of acid red 88. Sep Purif Technol 250:117232. https://doi.org/10.1016/j.seppur.2020.117232

Du X, Zhang Y, Si F, Yao C, Du M, Hussain I, Kim H, Huang S, Lin Z, Hayat W (2019) Persulfate non-radical activation by nano-CuO for efficient removal of chlorinated organic compounds: reduced graphene oxide-assisted and CuO (001) facet-dependent. Chem Eng J 356:178–189. https://doi.org/10.1016/j.cej.2018.08.216

Fan J, Qin H, Jiang S (2019) Mn-doped g-C_3N_4 composite to activate peroxymonosulfate for acetaminophen degradation: the role of superoxide anion and singlet oxygen. Chem Eng J 359:723–732. https://doi.org/10.1016/j.cej.2018.11.165

Fang G, Li J, Zhang C, Qin F, Luo H, Huang C, Qin D, Ouyang Z (2022) Periodate activated by manganese oxide/biochar composites for antibiotic degradation in aqueous system: combined effects of active manganese species and biochar. Environ Pollut 300:118939. https://doi.org/10.1016/j.envpol.2022.118939

Gaffar S, Dattamudi S, Baboukani AR, Chanda S, Novak JM, Watts DW, Wang C, Jayachandran K (2021) Physiochemical characterization of biochars from six feedstocks and their effects on the sorption of atrazine in an organic soil. Agronomy 11:716

Gasic S, Budimir M, Brkic D, Neskovic N (2002) Residues of atrazine in agricultural areas of Serbia. J Serb Chem Soc 67:887–892. https://doi.org/10.2298/jsc0212887g

Giannakopoulos S, Frontistis Z, Vakros J, Poulopoulos SG, Manariotis ID, Mantzavinos D (2022) Combined activation of persulfate by biochars and artificial light for the degradation of sulfamethoxazole in aqueous matrices. J Taiwan Inst Chem Eng 136:104440. https://doi.org/10.1016/j.jtice.2022.104440

Han D, Wan J, Ma Y, Wang Y, Li Y, Li D, Guan Z (2015) New insights into the role of organic chelating agents in Fe(II) activated persulfate processes. Chem Eng J 269:425–433. https://doi.org/10.1016/j.cej.2015.01.106

Hao H, Zhang Q, Qiu Y, Meng L, Wei X, Sang W, Tao J (2020) Insight into the degradation of Orange G by persulfate activated with biochar modified by iron and manganese oxides: synergism between Fe and Mn. J Water Process Eng 37:101470. https://doi.org/10.1016/j.jwpe.2020.101470

He L, Shi Y, Chen Y, Shen S, Xue J, Ma Y, Zheng L, Wu L, Zhang Z, Yang L (2022) Iron-manganese oxide loaded sludge biochar as a novel periodate activator for thiacloprid efficient degradation over a wide pH range. Sep Purif Technol 288:120703. https://doi.org/10.1016/j.seppur.2022.120703

Jiang M, Lu J, Ji Y, Kong D (2017) Bicarbonate-activated persulfate oxidation of acetaminophen. Water Res 116:324–331. https://doi.org/10.1016/j.watres.2017.03.043

Jiang Z, Li J, Jiang D, Gao Y, Chen Y, Wang W, Cao B, Tao Y, Wang L, Zhang Y (2020) Removal of atrazine by biochar-supported zero-valent iron catalyzed persulfate oxidation: reactivity, radical production and transformation pathway. Environ Res 184:109260. https://doi.org/10.1016/j.envres.2020.109260

Kolekar PD, Patil SM, Suryavanshi MV, Suryawanshi SS, Khandare RV, Govindwar SP, Jadhav JP (2019) Microcosm study of atrazine bioremediation by indigenous microorganisms and cytotoxicity of biodegraded metabolites. J Hazard Mater 374:66–73. https://doi.org/10.1016/j.jhazmat.2019.01.023

Leichtweis J, Silvestri S, Carissimi E (2020) New composite of pecan nutshells biochar-ZnO for sequential removal of acid red 97 by adsorption and photocatalysis. Biomass Bioenergy 140:05648. https://doi.org/10.1016/j.biombioe.2020.05648

Li B, Yang L, Wang CQ, Zhang QP, Liu QC, Li YD, Xiao R (2017a) Adsorption of Cd(II) from aqueous solutions by rape straw biochar derived from different modification processes. Chemosphere 175:332–340. https://doi.org/10.1016/j.chemosphere.2017.02.061

Li Y, Zhu Y, Liu X, Wu X, Dong F, Xu J, Zheng Y (2017b) Bioavailability assessment of thiacloprid in soil as affected by biochar. Chemosphere 171:185–191. https://doi.org/10.1016/j.chemosphere.2016.12.071

Li J, Guo Z, Cui K, Chen X, Yang X, Dong D, Xi S, Wu Z, Wu F (2023) Remediating thiacloprid-contaminated soil utilizing straw biochar-loaded iron and manganese oxides activated persulfate: removal effects and soil environment changes. J Hazard Mater 459:132066. https://doi.org/10.1016/j.jhazmat.2023.132066

Liang J, Duan XG, Xu XY, Chen KX, Zhang Y, Zhao L, Qiu H, Wang SB, Cao XD (2021) Persulfate oxidation of sulfamethoxazole by magnetic iron-char composites via nonradical pathways: Fe(IV) versus surface-mediated electron transfer. Environ Sci Technol 55:10077–10086. https://doi.org/10.1021/acs.est.1c01618

Liang Y, Ding LN, Song Q, Zhao B, Wang SY, Liu S (2022) Biodegradation of atrazine by three strains: identification, enzymes activities, and biodegradation mechanism. Environ Pollut Bioaval 34:549–563. https://doi.org/10.1080/26395940.2022.2151515

Liang J, Xu X, Zhong Q, Xu Z, Zhao L, Qiu H, Cao X (2020) Roles of the mineral constituents in sludge-derived biochar in persulfate activation for phenol degradation. J Hazard Mater 398:122861. https://doi.org/10.1016/j.jhazmat.2020.122861

Luo Z, Tu Y, Li H, Qiu B, Liu Y, Yang Z (2019) Endocrine-disrupting compounds in the Xiangjiang River of China: spatio-temporal distribution, source apportionment, and risk assessment. Ecotoxicol Environ Saf 167:476–484. https://doi.org/10.1016/j.ecoenv.2018.10.053

Luo J, Yi Y, Ying G, Fang Z, Zhang Y (2022) Activation of persulfate for highly efficient degradation of metronidazole using Fe(II)-rich potassium doped magnetic biochar. Sci Total Environ 819:152089. https://doi.org/10.1016/j.scitotenv.2021.152089

Milh H, Yu X, Cabooter D, Dewil R (2021) Degradation of ciprofloxacin using UV-based advanced removal processes: comparison of persulfate-based advanced oxidation and sulfite-based advanced reduction processes. Sci Total Environ 764:144510. https://doi.org/10.1016/j.scitotenv.2020.144510

Pan Y, Peng Z, Liu Z, Shao B, Liang Q, He Q, Wu T, Zhang X, Zhao C, Liu Y, Ge L, He M (2022) Activation of peroxydisulfate by bimetal modified peanut hull-derived porous biochar for the degradation of tetracycline in aqueous solution. J Environ Chem Eng 10:107366. https://doi.org/10.1016/j.jece.2022.107366

Panahi HKS, Dehhaghi M, Ok YS, Nizami AS, Khoshnevisan B, Mussatto SI, Aghbashlo M, Tabatabaei M, Lam SS (2020) A comprehensive review of engineered biochar: production, characteristics, and environmental applications. J Cleaner Prod 270:122462. https://doi.org/10.1016/j.jclepro.2020.122462

Peiris C, Gunatilake SR, Mlsna TE, Mohan D, Vithanage M (2017) Biochar based removal of antibiotic sulfonamides and tetracyclines in aquatic environments: a critical review. Bioresour Technol 246:150–159. https://doi.org/10.1016/j.biortech.2017.07.150

Qin F, Peng Y, Song G, Fang Q, Wang R, Zhang C, Zeng G, Huang D, Lai C, Zhou Y, Tan X, Cheng M, Liu S (2020) Degradation of sulfamethazine by biochar-supported bimetallic oxide/persulfate system in natural water: performance and reaction mechanism. J Hazard Mater 398:122816. https://doi.org/10.1016/j.jhazmat.2020.122816

Qu J, Li Z, Bi F, Zhang X, Zhang B, Li K, Wang S, Sun M, Ma J, Zhang Y (2023) A multiple Kirkendall strategy for converting nanosized zero-valent iron to highly active Fenton-like catalyst for organics degradation. Proc Natl Acad Sci USA 120:e2304552120. https://doi.org/10.1073/pnas.2304552120

Qu J, Xue J, Sun M, Li K, Wang J, Zhang G, Wang L, Jiang Z, Zhang Y (2024) Superefficient non-radical degradation of benzo[a]pyrene in soil by Fe-biochar composites activating persulfate. Chem Eng J 481:148585. https://doi.org/10.1016/j.cej.2024.148585

Shafizadeh A, Shahbeik H, Rafiee S, Moradi A, Shahbaz M, Madadi M, Li C, Peng WX, Tabatabaei M, Aghbashlo M (2023) Machine learning-based characterization of hydrochar from biomass: Implications for sustainable energy and material production. Fuel 347:128467. https://doi.org/10.1016/j.fuel.2023.128467

Shan R, Han J, Gu J, Yuan H, Luo B, Chen Y (2020) A review of recent developments in catalytic applications of biochar-based materials. Resour Conserv Recycl 162:105036. https://doi.org/10.1016/j.resconrec.2020.105036

Ta N, Hong J, Liu TF, Sun C (2006) Degradation of atrazine by microwave-assisted electrodeless discharge mercury lamp in aqueous solution. J Hazard Mater 138:187–194. https://doi.org/10.1016/j.jhazmat.2006.05.050

Tian SQ, Qi JY, Wang YP, Liu YL, Wang L, Ma J (2021) Heterogeneous catalytic ozonation of atrazine with Mn-loaded and Fe-loaded biochar. Water Res 193:116860. https://doi.org/10.1016/j.watres.2021.116860

Vonberg D, Hofmann D, Vanderborght J, Lelickens A, Köppchen S, Pütz T, Burauel P, Vereecken H (2014) Atrazine soil core residue analysis from an agricultural field 21 years after its ban. J Environ Qual 43:1450–1459. https://doi.org/10.2134/jeq2013.12.0497

Wang Z, Xiao F, Shen X, Zhang D, Chu W, Zhao H, Zhao G (2022) Electronic control of traditional iron-carbon electrodes to regulate the oxygen reduction route to scale up water purification. Environ Sci Technol 56:13740–13750. https://doi.org/10.1021/acs.est.2c03673

Wu S, He H, Li X, Yang C, Zeng G, Wu B, He S, Lu L (2018) Insights into atrazine degradation by persulfate activation using composite of nanoscale zero-valent iron and graphene: performances and mechanisms. Chem Eng J 341:126–136. https://doi.org/10.1016/j.cej.2018.01.136

Xiao R, Luo Z, Wei Z, Luo S, Spinney R, Yang W, Dionysiou DD (2018) Activation of peroxymonosulfate/persulfate by nanomaterials for sulfate

radical-based advanced oxidation technologies. Curr Opin Chem Eng 19:51–58. https://doi.org/10.1016/j.coche.2017.12.005
Xu R, Li M, Zhang Q (2022a) Collaborative optimization for the performance of ZnO/biochar composites on persulfate activation through plant enrichment-pyrolysis method. Chem Eng J 429:132294. https://doi.org/10.1016/j.cej.2021.132294
Xu S, Wen L, Yu C, Li S, Tang J (2022b) Activation of peroxymonosulfate by MnFe2O4@BC composite for bisphenol A degradation: the coexisting of free-radical and non-radical pathways. Chem Eng J 442:136250. https://doi.org/10.1016/j.cej.2022.136250
Xu Z, Sun M, Xu X, Cao X, Ippolito JA, Mohanty SK, Ni BJ, Xu S, Tsang DCW (2023) Electron donation of Fe-Mn biochar for chromium(VI) immobilization: key roles of embedded zero-valent iron clusters within iron-manganese oxide. J Hazard Mater 456:131632. https://doi.org/10.1016/j.jhazmat.2023.131632
Yan H, Huang S, Scholz M (2015) Kinetic processes of acute atrazine toxicity to Brachydanio rerio in the presence and absence of suspended sediments. Water Air Soil Pollut. 226:1–13. https://doi.org/10.1007/s11270-015-2296-7
Yang X, Xu G, Yu H, Zhang Z (2016) Preparation of ferric-activated sludge-based adsorbent from biological sludge for tetracycline removal. Bioresour Technol 211:566–573. https://doi.org/10.1016/j.biortech.2016.03.140
Yang Q, Wang X, Luo W, Sun J, Xu Q, Chen F, Zhao J, Wang S, Yao F, Wang D, Li X, Zeng G (2018) Effectiveness and mechanisms of phosphate adsorption on iron-modified biochars derived from waste activated sludge. Bioresour Technol 247:537–544. https://doi.org/10.1016/j.biortech.2017.09.136
Yang F, Zhang S, Cho DW, Du Q, Song J, Tsang DCW (2019) Porous biochar composite assembled with ternary needle-like iron-manganese-sulphur hybrids for high-efficiency lead removal. Bioresour Technol 272:415–420. https://doi.org/10.1016/j.biortech.2018.10.068
Zhang X, Li Y, Wu M, Pang Y, Hao Z, Hu M, Qiu R, Chen Z (2021a) Enhanced adsorption of tetracycline by an iron and manganese oxides loaded biochar: kinetics, mechanism and column adsorption. Bioresour Technol 320:124264. https://doi.org/10.1016/j.biortech.2020.124264
Zhang Y, Jiang Q, Jiang S, Li H, Zhang R, Qu J, Zhang S, Han W (2021b) One-step synthesis of biochar supported nZVI composites for highly efficient activating persulfate to oxidatively degrade atrazine. Chem Eng J 420:129868. https://doi.org/10.1016/j.cej.2021.129868
Zhu JF, Wang H, Duan A, Wang Y (2023) Mechanistic insight into the degradation of ciprofloxacin in water by hydroxyl radicals. J Hazards Mater 446:130676. https://doi.org/10.1016/j.jhazmat.2022.130676